Biochemical and Structural Evaluation of Highly Selective 2-Arylbenzoxazole-Based Transthyretin Amyloidogenesis Inhibitors

Steven M. Johnson,[†] Stephen Connelly,[‡] Ian A. Wilson,[‡] and Jeffery W. Kelly*,[†]

Departments of Chemistry and Molecular Biology, and The Skaggs Institute of Chemical Biology, The Scripps Research Institute, BCC 265, 10550 North Torrey Pines Road, La Jolla, California 92037

Received July 19, 2007

To develop potent transthyretin (TTR) amyloidogenesis inhibitors that also display high binding selectivity in blood, it proves useful to systematically optimize each of the three substructural elements that comprise a typical inhibitor: the two aryl rings and the linker joining them. In the first study, described herein, structural modifications to one aryl ring were evaluated by screening a library of 2-arylbenzoxazoles bearing thyroid hormone-like aryl substituents on the 2-aryl ring. Several potent and highly selective amyloidogenesis inhibitors were identified that exhibit minimal thyroid hormone nuclear receptor and COX-1 binding. High resolution crystal structures (1.3–1.5 Å) of three inhibitors (**2f**, **4f**, and **4d**) in complex with TTR were obtained to characterize their binding orientation. Collectively, the results demonstrate that thyroid hormone-like substitution patterns on one aryl ring lead to potent and highly selective TTR amyloidogenesis inhibitors that lack undesirable thyroid hormone receptor or COX-1 binding.

Introduction

Transthyretin (TTR[a]) is one of more than 25 disease-associated secreted human proteins that misfolds and misassembles into a variety of extracellular aggregate morphologies, including fibrillar cross-β-sheet structures known as amyloid. The native, tetrameric structure of TTR must first dissociate for the resulting monomers to partially unfold and misassemble into aggregates, including amyloid.[1,2] Substantial genetic and biochemical evidence link the process of TTR amyloid formation (amyloidogenesis), involving numerous assembly intermediates of variable morphology, to the tissue degeneration, including neurodegeneration, prevalent in senile systemic amyloidosis (SSA), familial amyloid cardiomyopathy (FAC), familial amyloid polyneuropathy (FAP), and central nervous system selective amyloidosis (CNSA).[1,3–6] FAP, FAC, and CNSA are familial diseases caused by the aberrant amyloidogenesis of one of >100 destabilized TTR mutants. These diseases can present as early as the second decade of life but typically present in the fourth to fifth decade. In contrast, SSA is a late onset disease associated with aggregation of wild type transthyretin (WT-TTR), typically presenting in the seventh to eighth decade. Without treatment, the TTR amyloidoses are fatal.

The liver secretes TTR into the blood, which later is envisioned to undergo amyloidogenesis. The only treatment currently available for FAP is gene therapy mediated by liver transplantation, whereby the FAP mutant TTR/WT-TTR secreting liver is replaced by a WT-TTR/WT-TTR secreting liver. This procedure dramatically decreases plasma mutant TTR levels and halts disease progression in most patients, at least initially.[7–9] In addition to the requirement for life-long immune suppression, another drawback of this strategy is that WT-TTR deposition often continues post-transplantation in the heart, leading to cardiomyopathy.[10] Liver transplantation is not envisioned to be effective for the treatment of SSA because this disease is caused by WT-TTR deposition. Because of these limitations, an alternative, generally applicable, oral small molecule therapy for all the TTR-based amyloid diseases is highly desirable.[4]

Transthyretin transports the vitamin A−retinol binding protein (RBP) complex and thyroxine (T_4) in blood. Because of the high concentration of TTR and the presence of two other thyroxine carrier proteins (thyroxine binding globulin and albumin), <1% of the thyroxine binding sites in the TTR tetramers are bound to T_4. TTR is composed of 127-amino acid, β-sheet-rich subunits that associate into a homotetrameric quaternary structure exhibiting two unique dimer–dimer interfaces (Figure 1).[4,11–15] The energetically weaker interface creates two funnel-shaped thyroxine binding pockets. Allosteric communication between the two binding sites causes thyroxine to bind with negative cooperativity, the structural basis of which is not entirely clear.[4,16,17] Each T_4 binding site contains three pairs of symmetric hydrophobic depressions, referred to as the halogen binding pockets (HBPs), wherein the iodine atoms of T_4 reside (Figure 1).[18] One pair is located in each of the smaller inner and larger outer binding cavities, while the third is found at the interface between the two cavities.

Numerous small molecules, typically composed of two differentially substituted aromatic rings connected by linkers of variable chemical composition (Figure 2), are known to avidly bind to the unoccupied T_4 sites within TTR (displaying either positive-, non-, or negative-cooperativity).[4] One aryl ring typically bears polar substituents that enable electrostatic interactions with the Lys-15 ϵ-NH_3^+ and/or the Glu-54 carboxy groups positioned at the periphery of the outer cavity of the T_4 binding site. Alternatively, these groups can hydrogen bond with the Ser-117 or Thr-119 hydroxyls in the inner cavity when bound in the opposite binding orientation. The other aryl substructure generally displays halogen or alkyl substituents that

* To whom correspondence should be addressed. Tel.: 858-784-9605. Fax: 858-784-9610. E-mail: jkelly@scripps.edu.

[†] Department of Chemistry.

[‡] Molecular Biology.

[a] Abbreviations: TTR, transthyretin; COX-1, cyclooxygenase-1; SSA, senile systemic amyloidosis; FAC, familial amyloid cardiomyopathy; FAP, familial amyloid polyneuropathy; CNSA, central nervous system amyloidosis; RBP, retinol binding protein; HBP, halogen binding pocket; PGE_2, prostaglandin E_2; T_4, thyroxine; T_3, triiodothyronine; NSAID, nonsteroidal, anti-inflammatory drug. PDB ascession codes: 2QGB, 2QGC, 2QGD, 2QGE.

10.1021/jm0708735 CCC: $40.75
Published on Web 12/21/2007

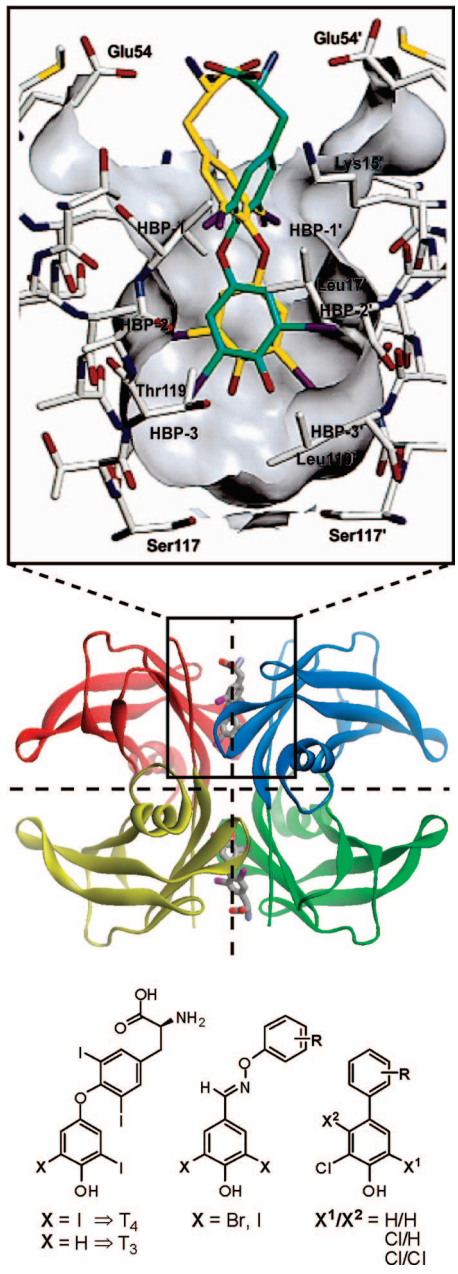

Figure 1. Crystal structure (2ROX) of thyroxine (T_4) bound within the two pockets created by the weak dimer–dimer interface of tetrameric TTR (the two dimer–dimer interfaces are represented by the dashed lines).[18] The expanded view of one site shows T_4 bound in its symmetry-related binding modes (green and yellow), with the binding site surface shown in gray (figure adapted from ref 18). Primed amino acids or halogen binding pockets (HBPs) refer to symmetry-related monomers of TTR. Two structural series of inhibitors are shown above, the bisaryloxime ethers and biphenyls (R = variable substitution patterns of fluorine, chlorine, trifluoromethyl, carboxyl, or hydroxyl substituents), many of which are excellent TTR kinetic stabilizers that display high plasma TTR binding selectivity.[25]

complement the hydrophobic HBPs positioned in the inner or outer cavities of the T_4 binding sites.

Small molecule binding to the T_4 sites can noncovalently bridge neighboring monomeric subunits via specific hydrophobic and electrostatic interactions, stabilizing the weaker dimer–dimer interface (Figure 1). This imposes kinetic stability on the native quaternary structure of TTR, precluding rate-limiting tetramer dissociation and, hence, amyloidogenesis from commencing.[4,13,15,19,20] Because genetic studies have uncovered a mechanistically analogous strategy that prevents human disease,

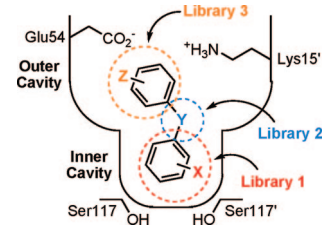

Figure 2. Schematic depiction of one of the two T_4 binding pockets within TTR occupied by a typical small molecule TTR aggregation inhibitor. Y represents a linker of variable chemical structure (e.g., NH, O, CH=CH, C(O)NH, etc.) joining the two aryl rings, which typically bear a combination of alkyl, carboxyl, halide, trifluoromethyl, or hydroxyl substituents (X and Z). Library 1, being the focus of this manuscript, explores the SAR of the aryl-X substructure.

there is good reason to be optimistic that small molecule TTR kinetic stabilizers will be efficacious against TTR amyloid disease. This strategy, called interallelic *trans*-suppression, is observed in compound heterozygotes having one allele coding for the disease-associated V30M-TTR variant (associated with high FAP penetrance) and the other allele coding for T119M-TTR. Inclusion of T119M subunits into heterotetramers otherwise composed of V30M subunits kinetically stabilizes TTR, preventing tetramer dissociation, amyloidogenesis, and the onset of FAP symptoms.[4,19,21–23] Besides demonstrating the efficacy of kinetic stabilization for ameliorating transthyretin amyloid disease, this data provides strong evidence for the amyloid hypothesis as the basis for pathology, that is, the notion that TTR dissociation, misfolding, and misassembly cause the TTR amyloidoses.[23]

The efficacy of candidate small molecule transthyretin amyloidogenesis inhibitors is typically evaluated by using a simple turbidity assay (turbidity increases with protein aggregation). Screening and structure-based drug design have enabled the evaluation of more than 650 candidate TTR amyloidogenesis inhibitors.[4,18,20,24–36] Of these, $\sim^1/_3$ are potent inhibitors of acid-mediated aggregation of TTR in vitro (described in more detail below), that is, they allow $<10\%$ of the aggregation ($>90\%$ inhibition) exhibited by inhibitor-free control samples over a 72 h time course. Potent inhibition of TTR amyloidogenesis in vitro is necessary, but not sufficient, for efficacy in humans: the small molecule TTR kinetic stabilizers must also bind selectively to TTR over all of the other proteins in blood.[37] Of the $\sim$200 compounds exhibiting $>90\%$ inhibition of TTR amyloidogenesis in vitro, only $\sim^1/_4$ of these display high binding selectivity in plasma (>1.0 out of a maximum of 2 equiv of inhibitor bound per tetramer).[37]

To develop an effective clinical candidate, it would be advantageous to have a number of structurally diverse, potent, and highly selective TTR kinetic stabilizers. The majority of the potent and selective TTR kinetic stabilizers are found in three structural families: bisaryloxime ethers, biphenyls, and 1-aryl-4,6-biscarboxydibenzofurans ($\sim$20, 30, and 40%, respectively); the remaining 10% are based on 2-phenylbenzoxazole or biphenylamine substructures.[18,25,27,31–33,36] Unfortunately, many of the most potent and selective bisaryloxime ethers have lower than desirable chemical stability,[25] leaving the biphenyls and dibenzofuran inhibitors as primary candidates. The lack of selective, structurally diverse clinical candidates is in large part due to the fact that there has been no systematic optimization of the three structural elements composing a typical small molecule TTR amyloidogenesis inhibitor, that is, the two variably substituted aromatic rings and the linker joining them (Figure 2). Consequently, we have developed three small

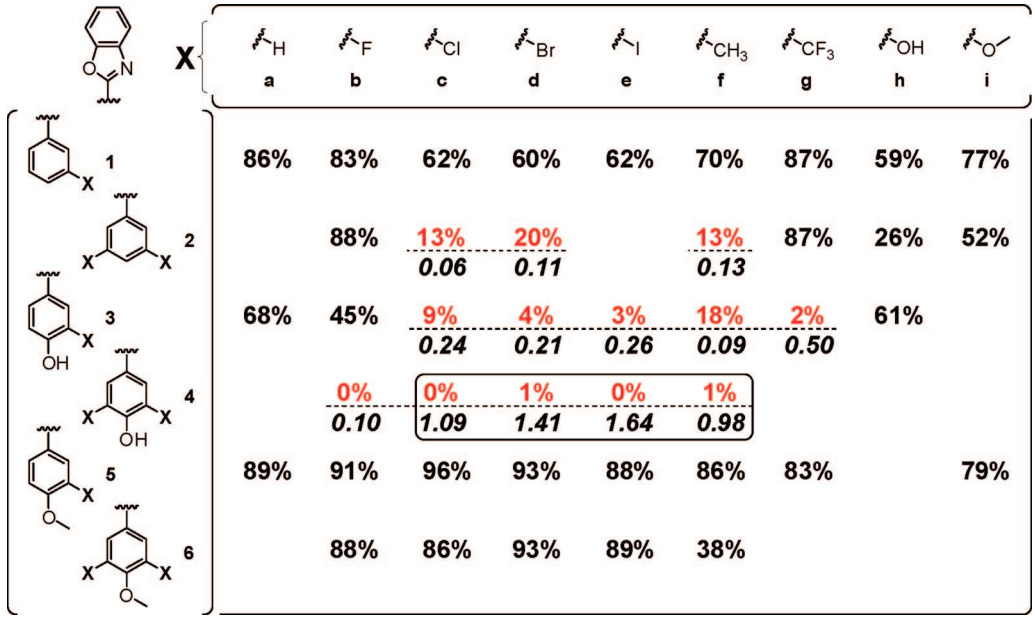

Figure 3. Inhibition of TTR aggregation and stoichiometry of benzoxazole bound to TTR in human blood plasma. Percent (%) values represent the extent of in vitro WT-TTR fibril formation in the presence of inhibitor (7.2 μM inhibitor, 3.6 μM TTR, pH 4.4, 37 °C, 72 h) relative to aggregation in the absence of inhibitor (100%), with the best values shown in red (<20% aggregation; errors are typically less than ±5 percentage points). The average stoichiometries of the most potent aggregation inhibitors bound to TTR in human blood plasma ex vivo are shown in italics (10.8 μM inhibitor, 1.8–5.4 μM TTR; maximum binding stoichiometry 2) with those exhibiting exceptional binding selectivity to TTR boxed (errors are typically less than ±0.1).

molecule libraries to systematically optimize these substructures to create potent and especially highly selective TTR amyloidogenesis inhibitors. The structure–activity relationship (SAR) data from these libraries will ultimately be utilized to predict the structures of diverse, potent, and highly selective TTR amyloidogenesis inhibitors, which should increase the chances of developing a successful clinical candidate.

The synthesis and evaluation of the first library, designed to optimize the aryl-X ring (Figure 2), is presented herein. In this exercise, the 2-aryl ring of an otherwise unsubstituted 2-arylbenzoxazole scaffold is modified with various substituents to evaluate the influence of thyroid hormone-like aryl substructures (3,4,5-substituted aryls, Figure 3) on transthyretin amyloidogenesis and selective binding to TTR in blood plasma. Because amelioration of transthyretin amyloidosis (SSA, FAP, and FAC) is envisioned to require life-long therapy with TTR small molecule kinetic stabilizers, it is essential that these drugs minimally interfere with other biological processes to mitigate toxicity. Therefore, we have further evaluated the potent TTR amyloidogenesis inhibitors identified here for their ability to bind to the nuclear thyroid hormone receptor, as well as inhibit cyclooxygenase-1 (COX-1) activity. Effective clinical candidates should be neither thyroid hormone agonists/antagonists, nor should they inhibit COX-1 enzymatic activity because FAP/FAC patients typically have amyloid deposition in the kidneys and gastro-intestinal tract, which compromises function and can be exacerbated by COX-1 inhibition.[38]

Herein, we report potent and highly selective TTR amyloidogenesis inhibitors bearing thyroid hormone-like substitution patterns on the aryl-X ring that, in general, do not bind to the COX-1 enzyme or the thyroid hormone receptor. Further evaluation by X-ray crystallography provides interesting insight into the structural basis for the ability of several of these potent inhibitors to bind to TTR.

Design and Synthesis. Previous studies reveal that 2,4,6-triiodophenol is a potent TTR amyloidogenesis inhibitor, which is impressive considering that potent inhibition generally requires two differentially substituted aryls connected by a linker.[4,18,20,24–36] It is also known that incorporation of the 3,5-dihalo-4-hydroxyphenyl substructure into bisaryloxime ether and biphenyl-based inhibitors (Figure 1, bottom) yields potent TTR amyloidogenesis inhibitors that exhibit selective binding to plasma TTR, almost irrespective of the substituents on the other aryl ring.[25,32] Collectively, these data suggest that it is likely that appending a 3,5-dihalo-4-hydroxyphenyl aryl ring, or a mimetic thereof, to a variety of molecules could render them potent and selective TTR kinetic stabilizers; hence, we focused on similar substituents and substitution patterns (Figure 3). Aryl rings substituted in this fashion were envisioned to interact within the inner cavity of the T_4 binding site (much like the analogous aryl ring in thyroxine, Figure 1). Optimization of the composition of the aryl-X ring will enable these aryl-X substructures to be utilized in future studies that seek ideal aryl-Z ring and linker-Y substructures (Figure 2). Data generated in this study can be combined with future analogous data on optimal aryl-Z and like substructures to predict the structures of exceptionally potent and selective TTR amyloidogenesis inhibitors.

In 2003, we demonstrated that 2-arylbenzoxazole-based compounds are potent TTR kinetic stabilizers in vitro that display the full range of binding selectivity in human plasma, affording stoichiometries from near zero to the theoretical maximum of two, depending on the substituents and substitution patterns on the 2-phenyl and benzoxazole substructures.[33] Therefore, substituting a variety of aryls at the 2-position of an otherwise unsubstituted benzoxazole scaffold should enable optimization of the aryl-X ring, as discussed above. A 42-member library of 2-arylbenzoxazole compounds, with variation in the 2-aryl ring, was synthesized as described previously (Scheme 1, Figure 3).[33,39] Compounds were characterized by

Scheme 1. General Synthesis of the Thyroid Hormone-Like 2-Arylbenzoxazoles[a]

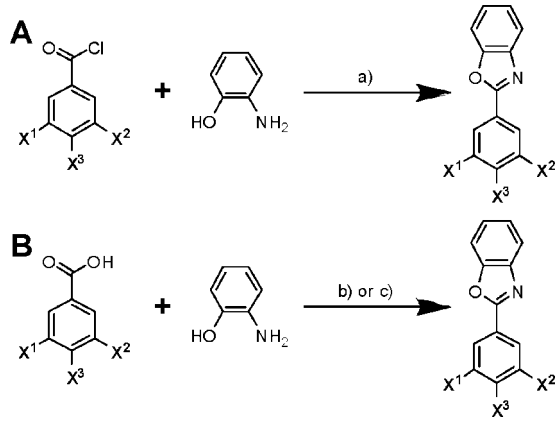

[a] (A) (a) pyridine, xylenes, rt, 1 h, then *p*-TsOH·H_2O added and refluxed. (B) (b) *p*-TsOH·H_2O, refluxing xylenes; (c) (i) *N*,*N*′-carbonyldiimidazole with $ArCO_2H$ in THF, 15 min, rt, then 2-aminophenol added and refluxed; (ii) *p*-TsOH·H_2O, refluxing xylenes. X^1 = H or X^2; X^2 = H, F, Cl, Br, I, CH_3, CF_3, OH, OCH_3; and X^3 = H, OH, OCH_3.

^{1}H and ^{13}C NMR spectroscopy, by mass spectrometry, and by RP-HPLC (all display >95% purity).

Results

Evaluating 2-Arylbenzoxazole-Mediated Inhibition of WT-TTR Amyloidogenesis. The ability of candidate 2-arylbenzoxazoles to inhibit WT-TTR amyloidogenesis was evaluated using the established acid-mediated aggregation assay.[40] Briefly, physiologically relevant concentrations of WT-TTR (3.6 μM) preincubated with a candidate inhibitor (7.2 μM) were subjected to partial denaturation under conditions that enable ~90% of WT-TTR to aggregate in the absence of inhibitor after 72 h (pH 4.4, 37 °C). The extent of aggregation is monitored by measuring sample turbidity, which has previously been demonstrated to be equivalent to monitoring amyloidogenesis by thioflavin-T fluorescence.[41] Inhibitor potency is expressed as % aggregation at the 72 h time point (compared to aggregation in the absence of inhibitor) with 0% aggregation equating to 100% inhibition. For the purposes here, we have defined a potent inhibitor as allowing <20% TTR aggregation; 13 compounds proved to be potent inhibitors of WT-TTR aggregation by this definition (Figure 3, red data). Although the series **1**, **5**, and **6** compounds are poor kinetic stabilizers of TTR, several compounds in the **2**−**4** series proved to be potent TTR amyloidogenesis inhibitors.

Binding Selectivity of Amyloidogenesis Inhibitors to TTR in Human Blood Plasma. The 13 potent 2-arylbenzoxazole aggregation inhibitors were further evaluated for their ability to bind selectively to TTR in the blood using the published ex vivo TTR plasma binding selectivity assay.[37] Briefly, the candidate 2-arylbenzoxazole (10.8 μM) is incubated in human blood plasma in the dark at 37 °C for 24 h. Transthyretin, with any bound inhibitor, is then captured by a resin-conjugated anti-TTR antibody and any unbound material is washed away (including weakly or nonspecifically bound inhibitors). The captured TTR·$(\text{inhibitor})_n$ complex is then dissociated from the antibody under alkaline conditions and quantified by RP-HPLC. The results represent the average stoichiometry of inhibitor bound per TTR tetramer (Figure 3, lower italicized values), the theoretical maximum being 2, owing to the two thyroxine binding sites. Of the 13 potent aggregation inhibitors evaluated, four display binding stoichiometries in excess of ~1 equiv bound per tetramer (**4c**−**f**), with the remainder displaying <0.5 equiv bound.

Inhibition of COX-1 Enzymatic Activity by the Potent TTR Amyloidogenesis Inhibitors. The 13 potent TTR aggregation inhibitors were further evaluated for their ability to inhibit the COX-1 enzyme (analyses that were contracted out to the Cerep laboratories in Redmond, WA). Compound analyses were performed using assay catalog reference #777-1 hr, which uses procedures developed by Glaser et al.[42] Briefly, the COX-1 enzyme (~2 μg in 250 μL of buffer) is preincubated in the absence or presence of test compound (10.0 μM) for 20 min at 22 °C. Arachidonic acid (4 μM) is then added, which undergoes catalytic conversion by COX-1 to afford prostaglandin-E_2 (PGE_2). After 10 min, the reaction is quenched by addition of 2 M HCl followed by 1 M Tris-HCl (pH 7.8) and cooling to 4 °C. PGE_2 is then quantified using an EIA detection kit. Results represent the % inhibition of arachidonic acid conversion to PGE_2 due to competitive binding of test compound to COX-1 (Figure 4, lower, black values). Of the 13 compounds evaluated, all but three display <5% inhibition of COX-1 activity, which is important to mitigate toxicity in the FAP/FAC patients for which inhibition of COX-1 enzymatic activity (anti-inflammatory agents) is contraindicated. Compounds **2d**, **2f**, and **4e** display 11–18% COX-1 inhibition.

Binding of TTR Amyloidogenesis Inhibitors to the Thyroid Hormone Nuclear Receptor. Because the compounds under investigation bear thyroid hormone-like 2-aryl substructures, the potent TTR amyloidogenesis inhibitors were further evaluated for their ability to interact with the thyroid hormone receptor (analyses that were contracted out to the Cerep laboratories in Redmond, WA). Compound analyses were performed using assay catalog reference #855, which uses procedures developed by Inoue et al.[43] Briefly, liver membrane homogenates (100 μg protein in 500 μL of buffer) were incubated for 18 h at 4 °C with 0.1 nM ^{125}I-labeled triiodothyronine ($[^{125}I]T_3$, the primary thyroid hormone, with a binding IC_{50} = 0.38 nM) in the absence or presence of test compound (10.0 μM). The samples were vacuum filtered through glass fiber filters, which were then rinsed several times with ice-cold buffer, dried, and counted for radioactivity. Nonspecific binding, determined in the presence of 1 μM T_3, is subtracted from the $[^{125}I]T_3$ binding results. Results represent the % displacement of $[^{125}I]T_3$ due to competitive binding of test compound to the thyroid hormone receptor (Figure 4, red, italicized values). Of the 13 compounds evaluated, all but one display insignificant (<5%) inhibition of T_3 binding to the thyroid hormone nuclear receptor, important for avoiding toxicity in the intended long-term use. Compound **4e** displays 17% inhibition of T_3 binding, a compound also displaying COX-1 binding capacity.

X-ray Crystallographic Analysis of WT-TTR Bound to Inhibitors 2f, 4d, and 4f. Crystal structures of *apo*-WT-TTR and TTR in complex with compounds **2f**, **4d**, and **4f** were determined to 1.4, 1.45, 1.5, and 1.3 Å resolutions, respectively. While the observed electron density for inhibitor **2f** was weaker, the electron density for the other two inhibitor-containing structures was clear and allowed unambiguous placement of the ligands. Inhibitors **2f** and **4f** bind in what is referred to as the "forward" mode, with their 3,5-dimethylphenyl and 3,5-dimethyl-4-hydroxyphenyl substructures, respectively, occupying the inner cavity of the thyroxine binding site (Figure 5). As such, their methyl substituents extend into the two halogen binding pockets located in the inner binding cavity (HBP-3 and 3′). In the **4f** structure, the Ser-117 and 117′ side chains of adjacent TTR subunits are bridged through hydrogen bonding with the

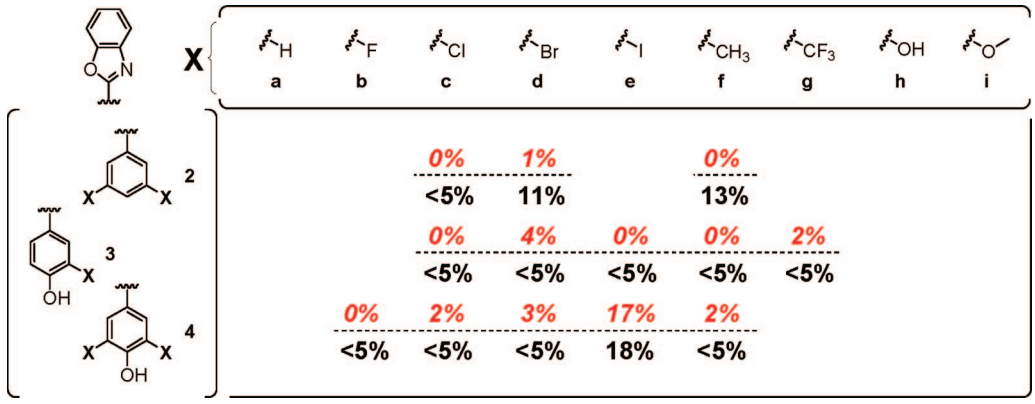

Figure 4. Thyroid hormone receptor binding and COX-1 inhibition data for the most potent TTR kinetic stabilizers. The extent of competitive inhibitor binding to the thyroid hormone receptor is shown in red italics, representing the % displacement of ^{125}I-labeled triiodothyronine (T_3, the primary thyroid hormone; errors are typically less than ±2 percentage points). COX-1 inhibition results are shown below in black, with values representing the % inhibition of COX-1 mediated conversion of arachidonic acid to prostaglandin-E_2 by the test compounds (errors are typically less than ±6 percentage points).

4-OH substituent of inhibitor **4f**. In the **2f** structure, an ordered water molecule replaces the missing phenolic group. In contrast to the forward binding mode exhibited by inhibitors **2f** and **4f**, inhibitor **4d** binds in the "reverse" binding mode, whereby its bromines extend into the outer cavity HBPs-1 and 1′ (Figure 5) and the phenolic substituent interacts with the Lys-15 and 15′ ϵ-NH_3^+ groups. In all three structures, the 2-aryl ring is bound rigidly in either the inner or outer cavities (**2f**/**4f** and **4d**, respectively), while occupancy by the benzoxazole rings show greater variability. Although ordered water molecules are present within each structure, these do not make any significant interactions with any of the bound inhibitors.

Discussion

Aryl Substructures Leading to Potent WT-TTR Aggregation Inhibitors. The specific interactions made by the rigidly positioned substituted 2-aryl rings (aryl-X) in the **2d**, **4d**, and **4f** amyloidogenesis inhibitor/TTR cocrystal structures likely contribute the most to the binding affinity and specificity, while the unsubstituted benzoxazole aromatic appears to contribute less. Although the potentially unpredictable binding orientations of the 2-arylbenzoxazoles complicate a detailed structure–activity relationship (SAR) interpretation, several trends are evident even in the absence of structural data for each ligand (Figure 3). Two dominant ligand−protein interactions contribute to inhibitor potency: the hydrophobic/electrostatic interactions of the 3,5-X_2 substituents and the electrostatic interactions of the 4-OH group. The most potent inhibitors, containing the thyroxine-like 3,5-X_2-4-OH 2-aryl substitution pattern (series **4**, Figure 3), enable both hydrophobic and electrostatic interactions.

The hydrophobicity of the 3,5-substituents is known to play a role in the binding affinity of ligands to transthyretin; increased hydrophobicity generally leads to increased binding affinity and, therefore, increased inhibitor potency.[44] Consistent with this interpretation, hydrogen and fluorine substituents tend to afford poorer aggregation inhibitors than their chloro, bromo, iodo, and methyl counterparts due to less-efficient interactions with the HBPs. Halogens are known to contribute more to ligand binding affinity than would be expected based on their hydrophobicity alone.[44,45] Formation of a charge-transfer complex between the halogen and a neighboring oxygen atom could be the basis for enhanced inhibitor binding.[44,45] Bis-*meta*-substitution appears superior to mono-*meta*-substitution, as exemplified by the increased potency of several of the series **2** (3,5-X_2) compounds over the series **1** compounds (3-X only). This effect may be a result of the 3,5-X_2 substituents being able to efficiently interact with two HBPs on adjacent TTR subunits simultaneously, whereas mono-*meta*-substitution enables occupancy of only one HBP and is, therefore, less efficient at stabilizing the weaker dimer–dimer interface.

The contribution of the 4-OH group (series **3** and **4**) to high binding affinity is emphasized by the increased potencies of the series **3** and **4** compounds over the series **1** and **2** compounds. The phenolic group can make hydrogen bonding interactions that bridge the Ser-117 and 117′ hydroxyls (Figure 5), as demonstrated in the **4f** cocrystal structure. The H-bonding enabled by **4f** leads to higher affinity relative to **2f**, which lacks a phenolic substituent, and is consistent with the weaker electron density for **2f** that results in higher *B*-values (Table 1). Interestingly, the isostructural compound **4d** binds in an orientation opposite to that of **4f**. In the TTR·(**4d**)$_2$ structure, the phenolic group can now engage in electrostatic interactions with the Lys-15 and 15′ ϵ-NH_3^+ groups. We posit that the binding orientation differences of **4d** and **4f** are caused by the different inductive effects of the bromine and methyl substituents. With **4f**, the electron-donating methyls result in a higher pK_a for the phenolic group, such that it is protonated (pK_a calcd to be 9.21; refer to Figure S2 in the Supporting Information),[46] favoring hydrogen bonding with the Ser-117 and 117′ hydroxyls. In contrast, the electron-withdrawing bromines of **4d** appear to afford the phenoxide ion (pK_a calcd tothe importance of phenol ionization. Interestingly, *O*-methylation of **4f** to give analogue **6f** does not cause such a dramatic decrease in activity, reflecting the fact that our preliminary explanation may be oversimplistic.

Aryl Substructures Conferring Selective Binding to TTR in Human Blood. 2-Arylbenzoxazoles that have the highest affinity for recombinant TTR in buffer are not necessarily the most selective TTR binders in the blood because binding to other prominent plasma proteins, such as albumin, is possible. An ideal clinical candidate should bind selectively to TTR in the blood to mitigate off-pathway toxicity. Therefore, the TTR binding selectivities of the 13 potent 2-arylbenzoxazole inhibitors displaying <20% fibril formation were evaluated using the previously established TTR binding selectivity assay. Since only the binding stoichiometry of the inhibitor to TTR is evaluated in this assay, we cannot comment on selectivity as it relates to inhibitor binding to other specific plasma proteins, which limits a detailed interpretation of the primary factors governing TTR binding selectivity.

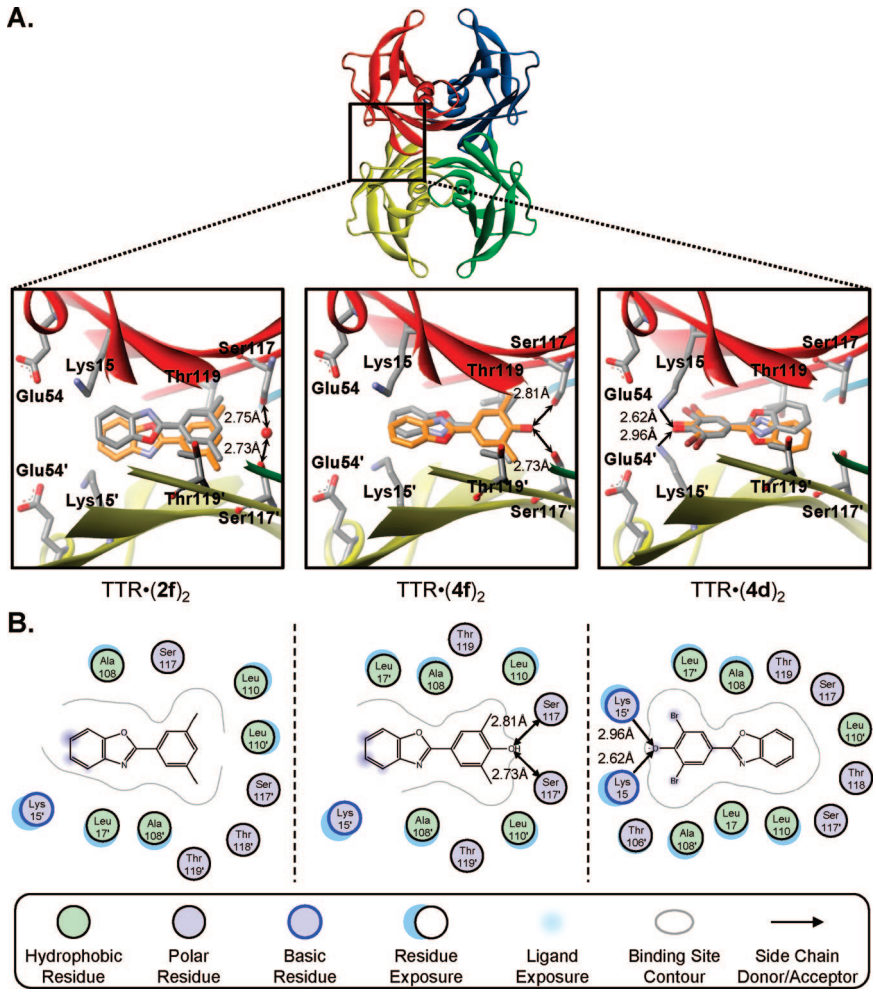

Figure 5. X-ray crystallographic structures of homotetrameric WT-TTR unliganded (PDB ascession code 2QGB) and cocrystallized with inhibitors **2f**, **4f**, and **4d** (PDB ascession codes 2QGE, 2QGC, and 2QGD, respectively). (A) Three-dimensional ribbon diagram of *apo*-TTR (top) with zoomed images of inhibitors **2f**, **4f**, and **4d** shown bound in one of the two symmetrical thyroxine binding sites. Individual TTR monomers have been colored red, yellow, green, and blue for differentiation. Inhibitors are shown bound in their two symmetry-related binding modes (orange and grey) and appear superimposed on one another due to their positioning on the crystallographic C_2 axis. The ordered water molecule bridging the Ser117 and 117′ hydroxyls of adjacent TTR monomers in the TTR•(**2f**)$_2$ structure is shown as a red sphere. Important hydrogen bonding and electrostatic interactions between residue side chains and the ligands (or H_2O as in the TTR•(**2f**)$_2$ structure) are indicated by arrows, with distance measurements in Å. (B) Schematic representation of the bound inhibitors as presented in panel **A** shown as two-dimensional topology diagrams (generated using MOE (2006.08), Chemical Computing Group, Montreal, Canada). Inhibitors have been shown in only one of their symmetry binding modes for clarity. A graphical legend for interpretation of key binding site characteristics is displayed below. Ligand exposure indicates specific portions of the ligand structures that are solvent accessible (i.e., not completely buried within the binding pocket). Residue exposure indicates those amino acids for which their side chains and/or peptide backbones are partially solvent accessible.

The 3,5-X_2-4-hydroxyphenyl substitution pattern (X = Cl, Br, I, and CH_3) in the series **4** inhibitors enables highly selective binding to TTR, with the exception of **4b**. These exemplary binding stoichiometries emphasize the synergistic interactions between the 3,5-X_2 and the 4-OH substituents, which enhance inhibitor binding affinity for reasons discussed above. That inhibitor binding affinity and selectivity can be further enhanced by adding substituents on the benzoxazole is encouraging for future lead development.[33]

Thyroid Hormone-Like 2-Arylbenzoxazoles Minimally Interact with the COX-1 Enzyme and the Thyroid Hormone Nuclear Receptor. To mitigate off-target toxicity, TTR small molecule kinetic stabilizers should not bind to COX-1 or the nuclear thyroid hormone receptor. Because many of these compounds resemble nonsteroidal, anti-inflammatory drugs (NSAIDs), which are contraindicated for treating FAP patients, we evaluated their COX-1 activity. The majority of the amyloidogenesis inhibitors display little, if any, inhibition of COX-1 activity (Figure 4, lower black entries).[42] The exceptions are compounds **2d**, **2f**, and **4e**, which display some COX-1 activity. The lack of COX-1 enzymatic inhibition by the majority of these compounds may be due to the absence of a carboxylate substituent, which is generally thought to be important for high affinity binding to the enzyme.[47–50]

Because the most potent 2-arylbenzoxazole TTR amyloidogenesis inhibitors have the 3-X-4-OH and 3,5-X_2-4-OH aryl substructures, as found in tri-iodothyronine (T_3, the primary thyroid hormone) and thyroxine (the prohormone), respectively, these were evaluated for their ability to interact with the nuclear thyroid hormone receptor. The T_3 competition binding assay indicates that, with the exception of **4e** (bearing the exact 3,5-I_2-4-hydroxyphenyl substitution pattern of thyroxine), the majority of the most potent TTR amyloidogenesis inhibitors do not interact significantly with the thyroid hormone receptor (Figure 4, red, italicized values).[43] The minimal thyroid hormone receptor binding is likely due to the lack of the carboxylic acid side chain that is present in T_3, which is important for polar interactions within the thyroid hormone receptor.[52–55] Additionally, the 3,5-X_2 aryl substitution pattern presumably decreases ligand binding affinity due to steric interaction of the 5-sub-

Table 1. Data Collection and Refinement Statistics for the Crystal Structures of TTR in *apo*-Form and in Complex with Inhibitors **2f**, **4d**, and **4f**

	apo-WT-TTR	WT-TTR/2f	WT-TTR/4d	WT-TTR/4f
Data Collection				
beamline	SSRL 11–1	SSRL 11–1	SSRL 11–1	SSRL 11–1
wavelength (Å)	0.9795	0.9795	0.9195	0.9795
resolution (Å)	1.40 (1.40–1.43)[a]	1.45 (1.45–1.50)	1.50 (1.50–1.53)	1.30 (1.30–1.35)
space group	$P2_12_12$	$P2_12_12$	$P2_12_12$	$P2_12_12$
a, *b*, *c* (Å)	42.85, 85.40, 64.35	42.92, 85.78, 64.56	42.95, 85.00, 65.10	43.00, 85.41, 64.42
No. of molecules in the a.u.	2	2	2	2
No. of observations	321624 (20703)	294859 (43361)	55736 (38439)	419806 (40887)
No. of unique reflections	47065 (3090)	42964 (6318)	38438 (2650)	59153 (5841)
completeness (%)	99.4 (100)	99.9 (100)	99.9 (100)	99.9 (100)
R_{sym} (%)[b]	4.5 (45.9)	4.0 (56.7)	6.2 (67.0)	3.6 (55.8)
avg I/σ	32.4 (4.2)	48.5 (3.4)	39.2 (4.5)	51.7 (3.8)
redundancy	6.8 (6.7)	6.9 (6.8)	14.5 (14.5)	7.1 (7.0)
Refinement Statistics				
resolution (Å)	1.40–64.42	1.45–64.55	1.50–65.09	1.30–64.42
No. of reflections (working set)	44643 (3009)	40759 (2926)	36456 (2491)	56119 (4033)
No. of reflections (test set)	2378 (174)	2163 (182)	1924 (122)	2986 (214)
R_{cryst} (%)[c]	16.6 (17.4)	16.4 (16.1)	15.9 (15.0)	15.4 (18.5)
R_{free} (%)[d]	18.8 (23.3)	20.0 (23.6)	19.9 (23.8)	17.4 (21.2)
No. TTR/ligands/water atoms	891884/0/166	891884/34/148	891884/34/142	891884/36/196
Average *B*-Values				
TTR	13.7	14.3	15.2	13.6
ligand	0	36.1	23.0	13.8
Wilson *B*-value	16.4	16.6	17.3	14.1
Ramachandran Plot				
most favored (%)	91.1	91.1	90.1	91.1
additionally allowed (%)	8.9	8.9	9.9	8.9
generously allowed (%)	0	0	0	0
disallowed (%)	0	0	0	0
R.M.S. Deviations				
bond lengths (Å)	0.019	0.019	0.019	0.019
angles (°)	1.83	1.78	1.76	1.72

[a] Numbers in parentheses are for highest resolution shell of data. [b] $R_{sym} = \Sigma_{hkl}|I - <I> \Sigma|_{hkl}\, I$. [c] $R_{cryst} = \Sigma_{hkl}|F_o - F_c|\Sigma_{hkl}F_o$. [d] R_{free} is the same as R_{cryst}, but for 5% of data excluded from the refinement.

stituent with residues in the thyroid hormone receptor binding site, as T_3 has a hydrogen in this position (Figure 1).[51–55]

Structural Insights for Development of Optimized TTR Amyloidogenesis Inhibitors. Although the thyroid hormone-like 2-aryl rings were envisioned to interact solely within the smaller inner cavity of the thyroxine binding sites, X-ray analysis demonstrates that this is not necessarily the case (Figure 5). Binding in either orientation permits energetically favorable interactions that noncovalently bridge and stabilize the adjacent TTR subunits across the weaker of the two dimer–dimer interfaces. Even though compounds **4d** and **4f** are both highly active and selective compounds, they exhibit strikingly different interactions throughout the outer and inner cavities of the T_4 binding site, respectively. When the TTR·(**4d**)$_2$ and TTR·(**4f**)$_2$ cocrystal structures are overlaid, the substituted phenyl substructures of each are reminiscent of the recently reported TTR·(PCB-OH)$_2$ cocrystal structure (Figure 6) in which the protein backbones, side chains, and the 3,5-X_2-4-hydroxyphenyl rings of the three structures superimpose nearly identically.[32] To our knowledge, PCB-OH is the most potent inhibitor discovered to date; it binds with the highest affinity (and relatively high selectivity) to TTR and is the only compound that displays positive binding cooperativity.[4,19,32,56,57] Because the 2-aryl rings of inhibitors **4d** and **4f** (i.e., the substituted phenyl rings) preferentially adopt conformations analogous to that observed in TTR·(PCB-OH)$_2$, these structures (TTR·(**4d**/**4f**)$_2$) should be valuable as templates to design inhibitors with optimal interactions in both the inner and outer cavities of the thyroxine binding sites.

Concluding Remarks. From this initial study that was designed to optimize the aryl-X substituents for transthyretin amyloidogenesis inhibitor potency and binding selectivity, we evaluated a library of 2-arylbenzoxazoles, of which 13 compounds potently inhibit TTR aggregation in vitro. Notably, four of these bind with high selectivity to transthyretin in blood plasma ex vivo. The most potent and selective inhibitors display little, if any, thyroid hormone nuclear receptor or COX-1 binding, which is highly desirable for transthyretin amyloidosis patients. The 3,4,5-substituted thyroxine-like aryl ring, but not necessarily the 3,5-I_2-4-hydroxyphenyl thyroxine aryl ring itself, appears to be an optimal solution for aryl-X ring composition for future studies, where subsequent libraries will be used to optimize the second ring (aryl-Z) and the linker for potency and binding selectivity. While X-ray crystallographic analysis demonstrates that incorporation of the 3,4,5-substituted aryl ring system into the 2-position of benzoxazoles does not necessarily guarantee a predictable binding orientation, we are optimistic that further studies for optimization of the linker and aryl-Z ring will provide more insight for predicting inhibitor binding orientations that can be verified by crystallographic analysis.

Experimental Section

General Synthetic Methods. Unless otherwise stated, all chemicals were purchased from commercial suppliers and used without further purification. Reaction progress was monitored by thin-layer chromatography on silica gel 60, F254-coated glass plates (EM Sciences). Flash chromatography was performed using 230–400 mesh silica gel 60 (EM Sciences). NMR spectra were recorded on a Bruker 500 MHz spectrometer. Chemical shifts are reported in parts per million downfield from the internal standard Me_4Si (0.0 ppm) for $CDCl_3$ solutions, and d_6-DMSO solutions were calibrated to the solvent peaks at 2.49 and 39.52 ppm for the ^1H and ^{13}C NMR spectra, respectively. Reverse phase high performance liquid chromatography (RP-HPLC) was performed using a Waters 600 E multisolvent delivery system employing a Waters 486 tunable

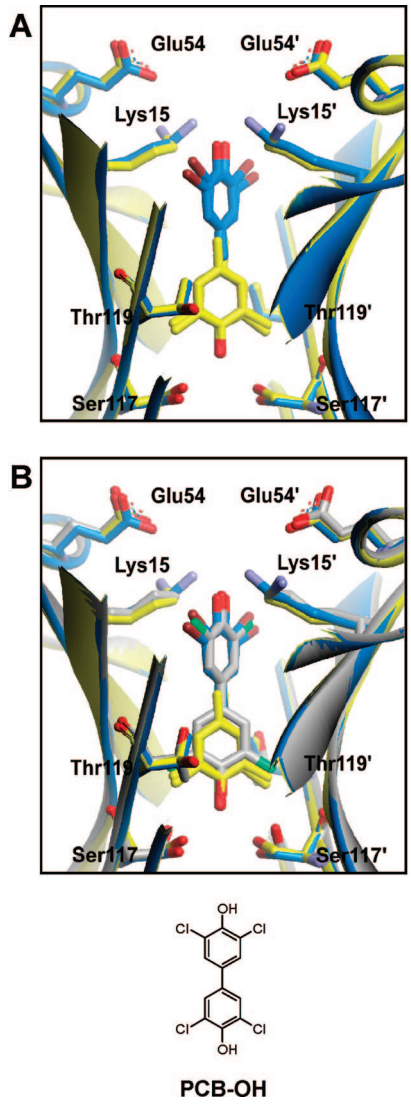

Figure 6. (A) Superimposition of the TTR·(**4d**)$_2$ and TTR·(**4f**)$_2$ crystal structures with the benzoxazole rings omitted for clarity. The protein backbones, residue side chains, and **4d** and **4f** inhibitors are displayed in blue and yellow, respectively. (B) Overlay of the resulting TTR·(**4d/f**)$_2$ hybrid and TTR·(PCB-OH)$_2$ crystal structures.[32] The protein backbones, residue side chains, and PCB-OH inhibitor of the TTR·(PCB-OH)$_2$ structure are displayed in grey for differentiation from the TTR·(**4d/f**)$_2$ hybrid structures as represented in panel A.

absorbance detector and 717 autosampler. Samples were chromatographically separated using a ThermoHypersil-Keystone Betabasic-18 column (model 71503–034630, 150 Å pore size, 3 μm particle size), eluting with a H_2O/CH_3CN gradient solvent system. Linear gradients were run from either 100:0, 80:20, or 60:40 A/B to 0:100 A/B (A = 95:5 H_2O/CH_3CN, 0.25% trifluoroacetic acid (TFA); B = 5:95 H_2O/CH_3CN, 0.25% TFA). Final compound purities were additionally evaluated under distinct RP-HPLC conditions by chromatographically separating samples using a Vydac-C_4 column (model 214TP5415, 300 Å pore size, 5 μm particle size), eluting with a H_2O/MeOH gradient solvent system. Linear gradients were run from 100:0 to 0:100 C/D (C = 99.75% H_2O, 0.25% TFA; D = 100% MeOH). All mass spectrometry data were collected at The Scripps Research Institute Center for Mass Spectrometry.

Representative Procedure for the Coupling of 2-Aminophenol with Substituted Benzoic Acids and Cyclodehydration to their Corresponding 2-Arylbenzoxazoles: Method A. Preparation of 2-(3-Chlorophenyl)benzoxazole (1c). 3-Chlorobenzoyl chloride (0.18 mL, 1.42 mmol), 2-aminophenol (125 mg, 1.15 mmol), and pyridine (94.0 μL, 1.15 mmol) were stirred in xylenes (10 mL) at room temperature for 1 h, then *p*-TsOH·H_2O (1.09 g, 5.75 mmol) was added and the reaction was stirred at reflux. After 4 h, the reaction was cooled, extracted into EtOAc (50 mL), and washed with saturated $NaHCO_3$ (2 × 25 mL) and brine (25 mL). The organics were then dried over Na_2SO_4, filtered, and concentrated. Flash chromatographic purification over silica (9:1 hexanes/EtOAc) afforded 2-(3-chlorophenyl)benzoxazole (**1c**) as a white solid (192 mg, 73%). ^{1}H NMR (500 MHz, $CDCl_3$) δ 8.25 (t, J = 1.8 Hz, 1H), 8.13 (dt, J = 1.4, 7.6 Hz, 1H), 7.75–7.80 (m, 1H), 7.56–7.61 (m, 1H), 7.50 (ddd, J = 1.3, 2.1, 8.0 Hz, 1H), 7.45 (dt, J = 0.3, 7.8 Hz, 1H), 7.35–7.39 (m, 2H); ^{13}C NMR (125 MHz, $CDCl_3$) δ 161.63, 150.79, 141.94, 135.09, 131.48, 130.22, 128.88, 127.62, 125.64, 125.54, 124.81, 120.24, 110.70; RP-HPLC 99% and 99% pure.

Please refer to the Supporting Information for specific synthetic details and characterization data for inhibitors prepared analogously.

Representative Procedure for the Coupling of 2-Aminophenol with Substituted Benzoic Acids and Cyclodehydration to their Corresponding 2-Arylbenzoxazoles: Method B. Preparation of 2-Phenylbenzoxazole (1a). 2-Phenylbenzoxazole (**1a**) was obtained from commercial sources and was also synthesized for method validation. Benzoic acid (111 mg, 0.909 mmol), 2-aminophenol (82.8 mg, 0.759 mmol), and *p*-TsOH·H_2O (720 mg, 3.79 mmol) were stirred in refluxing xylenes (10 mL). After 4 h, the reaction was cooled, extracted into EtOAc (50 mL), and washed with saturated $NaHCO_3$ (2 × 25 mL) and brine (25 mL). The organics were then dried over Na_2SO_4, filtered, and concentrated. Flash chromatographic purification over silica (9:1 hexanes/EtOAc) afforded 2-phenylbenzoxazole (**1a**) as a white solid (109 mg, 74%). ^{1}H and ^{13}C NMR were identical to the commercial sample. ^{1}H NMR (500 MHz, $CDCl_3$) δ 8.24–8.28 (m, 2H), 7.76–7.80 (m, 1H), 7.56–7.60 (m, 1H), 7.50–7.55 (m, 3H), 7.33–7.37 (m, 2H); ^{13}C NMR (125 MHz, $CDCl_3$) δ 163.05, 150.76, 142.11, 131.53, 128.92, 127.62, 127.17, 125.11, 124.59, 120.02, 110.60; RP-HPLC >99% and 99% pure.

Refer to the Supporting Information for specific synthetic details and characterization data for inhibitors prepared analogously.

Representative Procedure for the Coupling of 2-Aminophenol with Substituted Benzoic Acids and Cyclodehydration to their Corresponding 2-Arylbenzoxazoles: Method C. Preparation of 2-(3,5-Dibromophenyl)benzoxazole (2d). Modified procedures from Kumar et al. were employed.[39] 3,5-Dibromobenzoic acid (584 mg, 2.09 mmol) was added to a stirring solution of *N,N′*-carbonyldiimidazole (341 mg, 2.10 mmol) in anhydrous THF (20 mL) at room temperature under an argon atmosphere. After 15 min, the 2-aminophenol was added (194 mg, 1.78 mmol) and the reaction was stirred at reflux. After 18 h, the reaction was concentrated, then refluxed with *p*-TsOH·H_2O (1.70 g, 8.94 mmol) in *p*-xylene (18 mL). After 2 h, the reaction was cooled, extracted into EtOAc (100 mL), and washed with saturated $NaHCO_3$ (2 × 25 mL) and brine (25 mL). The organics were then dried over Na_2SO_4, filtered, and concentrated. Flash chromatographic purification over silica (100% hexanes to 9:1 hexanes/EtOAc gradient elution) afforded 2-(3,5-dibromophenyl)benzoxazole (**2d**) as a pale yellow solid (208 mg, 33%). ^{1}H NMR (500 MHz, $CDCl_3$) δ 8.34 (d, J = 1.7 Hz, 2H), 8.16 (t, J = 1.8 Hz, 1H), 7.77–7.80 (m, 1H), 7.58–7.61 (m, 1H), 7.37–7.43 (m, 2H); ^{13}C NMR (125 MHz, $CDCl_3$) δ 160.10, 150.84, 141.76, 136.70, 130.38, 129.13, 125.98, 125.06, 123.53, 120.45, 110.82; ESI-TOF m/z $[MH]^+$ calcd for $C_{13}H_8Br_2NO$, 351.8967; found, 351.8966; RP-HPLC 98% and 97% pure.

Please refer to the Supporting Information for specific synthetic details and characterization data for inhibitors prepared analogously.

Representative Procedure for the Methylation of Phenols. Preparation of 2-(3-Methoxyphenyl)benzoxazole (1i). 2-(3-Hydroxyphenyl)benzoxazole (**1h**, 29.6 mg, 0.140 mmol), iodomethane (17.5 μL, 0.281 mmol), and K_2CO_3 (39.3 mg, 0.284 mmol) were stirred in DMF (3 mL) at room temperature. After 18 h, the reaction was concentrated with silica to a powder. Flash chromatographic purification over silica (2:1 hexanes/EtOAc) afforded 2-(3-methoxyphenyl)benzoxazole (**1i**) as an amber solid (25.2 mg, 80%). ^{1}H NMR (500 MHz, $CDCl_3$) δ 7.85 (ddd, J =

1.0, 1.4, 7.7 Hz, 1H), 7.76–7.80 (m, 2H), 7.56–7.60 (m, 1H), 7.43 (t, $J = 8.0$ Hz, 1H), 7.33–7.38 (m, 2H), 7.08 (ddd, $J = 0.9$, 2.7, 8.3 Hz, 1H), 3.92 (s, 3H); ^{13}C NMR (125 MHz, $CDCl_3$) δ 162.98, 159.96, 150.77, 142.08, 130.01, 128.36, 125.17, 124.61, 120.14, 120.04, 118.36, 111.92, 110.61, 55.53; ESI-TOF *m/z* $[MH]^+$ calcd for $C_{14}H_{12}NO_2$, 226.0863; found, 226.0860; RP-HPLC 97% and 96% pure.

Refer to the Supporting Information for specific synthetic details and characterization data for inhibitors prepared analogously.

Representative Procedure for the Demethylation of Anisoles. Preparation of 2-(3,5-Dihydroxyphenyl)benzoxazole (2h). Boron tribromide (6.20 mL of 1 M BBr_3 in hexanes, 6.20 mmol) was added to a stirring mixture of **2i** (159 mg, 0.623 mmol) in anhydrous CH_2Cl_2 (6.0 mL), and the reaction was stirred at room temperature under an argon atmosphere. After 18 h, the reaction was quenched with MeOH (5 mL), extracted into EtOAc (50 mL), and washed with H_2O (2 × 25 mL) and brine (25 mL). The organics were then dried over Na_2SO_4, filtered, and concentrated. Flash chromatographic purification over silica (1:1 hexanes/EtOAc to 100% EtOAc gradient elution) afforded 2-(3,5-dihydroxyphenyl-)benzoxazole (**2h**) as an off-white solid (98.8 mg, 70%). ^{1}H NMR (500 MHz, d_6-DMSO) δ 9.74 (s, 2H), 7.74–7.79 (m, 2H), 7.36–7.43 (m, 2H), 7.06 (d, $J = 2.2$ Hz, 2H), 6.44 (d, $J = 2.2$ Hz, 1H); ^{13}C NMR (125 MHz, d_6-DMSO) δ 162.46, 159,03, 150.08, 141.45, 127.80, 125.37, 124.77, 119.73, 110.85, 106.10, 105.28; ESI-TOF *m/z* $[MH]^+$ calcd for $C_{13}H_{10}NO_3$, 228.0655; found, 228.0665; RP-HPLC 98% and 98% pure.

Refer to the Supporting Information for specific synthetic details and characterization data for inhibitors prepared analogously.

Evaluating Small Molecule-Mediated Inhibition of WT-TTR Amyloidogenesis. WT-TTR was purified from an *E. coli* expression system, as described previously.[58] To a 495 μL aliquot of 0.4 mg/mL WT-TTR (7.2μM, 10 mM phosphate, pH 7.0, 100 mM KCl, 1 mM EDTA) in a disposable cuvette was added 5 μL of a 1.44 mM DMSO solution of test compound and the sample was vortexed briefly. After incubating for 30 min at ambient temperature, the pH of the sample was lowered to 4.4 by the addition of 500 μL of acidic buffer (100 mM acetate, pH 4.2, 100 mM KCl, 1 mM EDTA), and the solution was briefly vortexed and incubated in the dark for 72 h at 37 °C (final protein and inhibitor concentrations were 3.6 and 7.2 μM, respectively). The sample was then vortexed to evenly distribute any precipitate, and the turbidity was measured at 400 nm on a Hewlett-Packard model 8453 UV–vis spectrophotometer. The extent of WT-TTR aggregation (% fibril formation, f.f.; % inhibition = 100 − %f.f.) was determined by comparing the sample turbidity in the presence of small molecule as a percentage of control WT-TTR sample incubated with 5 μL of pure DMSO (representing 100% aggregation, 0% inhibition). All samples were performed in at least triplicate, with average values obtained presented in Figure 3 (errors are typically less than ± 5 percentage points).

Evaluating the Binding Selectivity of Amyloidogenesis Inhibitors to TTR in Human Blood Plasma. The procedure for the antibody capture method to evaluate the stoichiometry of inhibitor bound to TTR in human blood plasma has been described in detail elsewhere.[37] Briefly, 7.50 μL of a 1.44 mM DMSO solution of test compound was incubated with human blood plasma (1 mL) in a 2 mL eppendorf tube in the dark at 37 °C for 24 h on a rocker (30 rpm). Then, 125 μL of a 1:1 v/v slurry of unfunctionalized sepharose resin in TSA (10 mM Tris, pH 8.0, 140 mM NaCl) was added, and the mixture was incubated for another hour at 4 °C on a rocker (18 rpm). The sample was then centrifuged, the supernatant was divided into 2 aliquots of 400 μL each, which were each added to 200 μL of a 1:1 v/v slurry of sepharose resin conjugated to an anti-TTR antibody in TSA, and the sample was incubated again at 4 °C for 20 min on a rocker (18 rpm). The sample was then centrifuged, the supernatant removed, and the TTR bound resin was washed three times (10 min each wash) with 1 mL of TSA/0.05% saponin, then twice (10 min each wash) with 1 mL TSA at 4 °C on a rocker (18 rpm). After centrifugation and removal of the final supernatant, dissociation of the TTR and bound test compound from the resin-bound antibody was achieved through addition of 155 μL of aqueous triethylamine (100 mM, pH ~ 11.5) and rocking (18 rpm) at 4 °C for 30 min. The suspension was then centrifuged, and 135 μL of the supernatant, containing both TTR and test compound, was analyzed by RP-HPLC to determine the stoichiometry of small molecule bound to TTR (the test compound−TTR complex dissociates and the small molecule and protein are chromatographically separable under the HPLC buffer conditions). Quantification of test compound and TTR is achieved by comparing the integrated peak areas to standard curves: the ratio of the amount of test compound to TTR yields the binding stoichiometry, of which a theoretical maximum value of 2 is possible due to the two T_4 binding sites per TTR tetramer. Analyses were performed in at least triplicates of duplicates from three different blood plasma samples (i.e., at least six analyses), with average values obtained presented in Figure 3 (errors are typically less than ±0.1).

Evaluating the Inhibition of COX-1 Enzymatic Activity by the Potent TTR Amyloidosis Inhibitors. The evaluation of the most potent TTR aggregation inhibitors (displaying <20% fibril formation) at inhibiting COX-1 activity was contracted out to the Cerep laboratories in Redmond, WA. Compound analyses were performed using assay catalog reference #777-1 hr, which uses procedures developed by Glaser et al.[42] A brief experimental protocol as provided by Cerep is outlined below. In this assay, the enzyme (~2 μg) is preincubated in the absence (water control) or presence of test compound (10.0 μM) for 20 min at 22 °C in 250 μL of buffer (100 mM Tris-HCl, pH 8, 2 mM phenol, 1 μM hematine). Arachidonic acid (4 μM) is then added to initiate the reaction (no arachidonic acid added for basal control measurements). After incubation at 22 °C for 10 min, the reaction is quenched by addition of 2 M HCl and 1 M Tris-HCl (pH 7.8) and cooling at 4 °C. Prostaglandin-E_2 (PGE_2) quantification is performed using an EIA detection kit, with measurements made using a microplate reader. Average values of duplicate analyses are presented in Figure 4 (black values), which represent the % inhibition of arachidonic acid conversion to PGE_2 due to competitive binding of test compound to COX-1 (errors of less than ± 6 percentage points are representative of the data). Control analyses are performed analogously with the standard inhibitory reference compound diclofenac tested at several concentrations to obtain an inhibition curve from which its IC_{50} is calculated (12 nM).

Evaluating the Binding of the Potent TTR Amyloidosis Inhibitors to the Thyroid Hormone Nuclear Receptor. The evaluation of the most potent TTR aggregation inhibitors (displaying <20% fibril formation) at binding to the thyroid hormone receptor was contracted out to the Cerep laboratories in Redmond, WA. Compound analyses were performed using assay catalog reference #855, which uses procedures developed by Inoue et al.[43] A brief experimental protocol as provided by Cerep is outlined below. In this assay, liver membrane homogenates (100 μg protein) are incubated for 18 h at 4 °C with 0.1 nM ^{125}I-labeled triiodothyronine ($[^{125}I]T_3$, the primary thyroid hormone) in the absence or presence of test compound (10.0 μM) in 500 μL of buffer (20 mM Tris-HCl, pH 7.6, 50 mM NaCl, 2 mM EDTA, 10% glycerol, and 5 mM β-mercaptoethanol). The samples are then vacuum filtered through glass fiber filters (GF/B, Packard), rinsed several times with ice-cold buffer (50 mM Tris-HCl and 150 mM NaCl), and the filters are dried and counted for radioactivity in a scintillation counter (Topcount, Packard) using a scintillation cocktail (Microscint 0, Packard). Nonspecific binding, determined in the presence of 1 μM T_3, is subtracted from the $[^{125}I]T_3$ binding results. Average values of duplicate analyses are presented in Figure 4 (red italicized values), which represent the % displacement of $[^{125}I]T_3$ due to competitive binding of test compound to the thyroid hormone receptor (errors of less than ± 2 percentage points are representative of the data). Control analyses are performed analogously with T_3 tested at several concentrations to obtain a competition curve from which its IC_{50} is calculated (0.38 nM).

X-ray Crystallographic Analysis of WT-TTR in *apo*-Form and Bound to Inhibitors 2f, 4d, and 4f. WT-TTR was purified from an *E. coli* expression system, as described previously.[58] The WT-TTR was concentrated to 4 mg/mL in 10 mM NaP_i, 100 mM KCl, at pH 7.6 and cocrystallized at room temperature with inhibitors **2d**, **4d**, and **4f** at a 5 M excess using the vapor-diffusion sitting drop method. Crystals were grown from 1.395 M sodium citrate, 3.5% v/v glycerol at pH 5.5. The crystals were cryoprotected with an inhibitor-free solution of 10% v/v glycerol. Data were collected at beam line 11-1 at the Stanford Synchrotron Radiation Laboratory (SSRL) at a wavelength of 0.9795 Å for the *apo*, **2f**, and **4f** crystals and at 0.9195 Å, corresponding to the bromine peak wavelength, for the **4d** crystals. The data sets were integrated and scaled using HKL2000.[59] The crystals were indexed in space group $P2_12_12$ with two subunits per asymmetric unit with unit cell dimensions $a = 84.9$ Å, $b = 43.9$ Å, and $c = 64.8$ Å. The four crystal structures were determined by molecular replacement using the model coordinates of 2FBR[60] in the program Phaser[61] to 1.4, 1.45, 1.5, and 1.3 Å resolutions for the *apo*, **2f**, **4d**, and **4f** structures, respectively. Further model building and refinement were completed using Refmac.[62] Hydrogens were added during refinement and anisotropic *B*-values were calculated. Final models were validated using the JCSG quality control server incorporating Molprobity,[63] ADIT (http://rcsb-deposit.rutgers.edu/validate) WHATIF,[64] Resolve,[65] and Procheck.[66] Data collection and refinement statistics are presented in Table 1.

Protein Data Bank Accession Codes. Atomic coordinates have been deposited in the RCSB Protein Data Bank (www.pdb.org) and are available under accession codes 2QGB (*apo*-form WT-TTR), 2QGE (WT-TTR in complex with **2f**), 2QGD (WT-TTR in complex with **4d**), and 2QGC (WT-TTR in complex with **4f**).

Acknowledgment. We are grateful for the financial support of the NIH DK 46335 (J.W.K), CA58896, and AI42266 (I.A.W.), as well as the Skaggs Institute of Chemical Biology and the Lita Annenberg Hazen Foundation. Assistance with the thyroid hormone receptor and COX-I binding assays by the Cerep laboratories (Redmond, WA, and France) and Richard Labaudiniere of FoldRx Pharmaceuticals (Boston, MA), as well as the technical expertise of Ted Foss, M. T. Dendle, and Mike Saure are also greatly appreciated. Portions of this research were carried out at the Stanford Synchrotron Radiation Laboratory, a national user facility operated by Stanford University on behalf of the U.S. Department of Energy, Office of Basic Energy Sciences. The SSRL Structural Molecular Biology Program is supported by the Department of Energy, Office of Biological and Environmental Research and by the National Institutes of Health, National Center for Research Resources, Biomedical Technology Program, and the National Institute of General Medical Sciences. The authors would also like to thank Drs. Robyn Stanfield, Xiaoping Dai, and Petra Verdino in the Wilson laboratory for assistance in data collection and structure determination.

Supporting Information Available: Detailed synthesis and characterization of the 2-arylbenzoxazoles and tabulation of compound purity as determined by RP-HPLC. This material is available free of charge via the Internet at http://pubs.acs.org.

References

(1) Reixach, N.; Deechongkit, S.; Jiang, X.; Kelly, J. W.; Buxbaum, J. N. Tissue damage in the amyloidoses: Transthyretin monomers and nonnative oligomers are the major cytotoxic species in tissue culture. *Proc. Natl. Acad. Sci. U.S.A.* **2004**, *101*, 2817–2822.

(2) Sekijima, Y.; Wiseman, R. L.; Matteson, J.; Hammarstrom, P.; Miller, S. R.; Sawkar, A. R.; Balch, W. E.; Kelly, J. W. The biological and chemical basis for tissue selective amyloid disease. *Cell* **2005**, *121*, 73–85.

(3) McCarthy, R. E.; Kasper, E. K. A review of the amyloidoses that infiltrate the heart. *Clin. Cardiol.* **1998**, *21*, 547–552.

(4) Johnson, S. M.; Wiseman, R. L.; Sekijima, Y.; Green, N. S.; Adamski-Werner, S. L.; Kelly, J. W. Native state kinetic stabilization as a strategy to ameliorate protein misfolding diseases: A focus on the transthyretin amyloidoses. *Acc. Chem. Res.* **2005**, *38*, 911–921.

(5) Jacobson, D. R.; Pastore, R. D.; Yaghoubian, R.; Kane, I.; Gallo, G.; Buck, F. S.; Buxbaum, J. N. Variant-sequence transthyretin (isoleucine 122) in late-onset cardiac amyloidosis in black Americans. *N. Engl. J. Med.* **1997**, *336*, 466–473.

(6) Plante-Bordeneuve, V.; Said, G. Transthyretin related familial amyloid polyneuropathy. *Curr. Opin. Neurol.* **2000**, *13*, 569–573.

(7) Holmgren, G.; Ericzon, B. G.; Groth, C. G.; Steen, L.; Suhr, O.; Andersen, O.; Wallin, B. G.; Seymour, A.; Richardson, S.; Hawkins, P. N. Clinical improvement and amyloid regression after liver transplantation in hereditary transthyretin amyloidosis. *Lancet* **1993**, *341*, 1113–1116.

(8) Tan, S. Y.; Pepys, M. B.; Hawkins, P. N. Treatment of amyloidosis. *Am. J. Kidney Dis.* **1995**, *26*, 267–285.

(9) Suhr, O. B.; Herlenius, G.; Friman, S.; Ericzon, B. G. Liver transplantation for hereditary transthyretin amyloidosis. *Liver Transplant.* **2000**, *6*, 263–276.

(10) Olofsson, B. O.; Backman, C.; Karp, K.; Suhr, O. B. Progression of cardiomyopathy after liver transplantation in patients with familial amyloidotic polyneuropathy, Portuguese type. *Transplantation* **2002**, *73*, 745–751.

(11) Blake, C. C.; Geisow, M. J.; Oatley, S. J.; Rerat, B.; Rerat, C. Structure of prealbumin: Secondary, tertiary and quaternary interactions determined by Fourier refinement at 1.8 A. *J. Mol. Biol.* **1978**, *121*, 339–356.

(12) Hornberg, A.; Eneqvist, T.; Olofsson, A.; Lundgren, E.; Sauer-Eriksson, A. E. A comparative analysis of 23 structures of the amyloidogenic protein transthyretin. *J. Mol. Biol.* **2000**, *302*, 649–669.

(13) Foss, T. R.; Kelker, M. S.; Wiseman, R. L.; Wilson, I. A.; Kelly, J. W. Kinetic stabilization of the native state by protein engineering: Implications for inhibition of transthyretin amyloidogenesis. *J. Mol. Biol.* **2005**, *347*, 841–854.

(14) Monaco, H. L.; Rizzi, M.; Coda, A. Structure of a complex of two plasma proteins: Transthyretin and retinol-binding protein. *Science* **1995**, *268*, 1039–1041.

(15) Foss, T. R.; Wiseman, R. L.; Kelly, J. W. The pathway by which the tetrameric protein transthyretin dissociates. *Biochemistry* **2005**, *44*, 15525–15533.

(16) Neumann, P.; Cody, V.; Wojtczak, A. Structural basis of negative cooperativity in transthyretin. *Acta Biochim. Pol.* **2001**, *48*, 867–875.

(17) Stockigt, J. R. Thyroid Hormone Binding and Metabolism. In *Endocrinology*, 4th edition; Degroot, L. J., Jameson, J. L., Eds.; W. B. Saunders Co.: Philadelphia, PA, 2001; pp 1314−1326.

(18) Klabunde, T.; Petrassi, H. M.; Oza, V. B.; Raman, P.; Kelly, J. W.; Sacchettini, J. C. Rational design of potent human transthyretin amyloid disease inhibitors. *Nat. Struct. Biol.* **2000**, *7*, 312–321.

(19) Hammarstrom, P.; Wiseman, R. L.; Powers, E. T.; Kelly, J. W. Prevention of transthyretin amyloid disease by changing protein misfolding energetics. *Science* **2003**, *299*, 713–716.

(20) Wiseman, R. L.; Johnson, S. M.; Kelker, M. S.; Foss, T.; Wilson, I. A.; Kelly, J. W. Kinetic stabilization of an oligomeric protein by a single ligand binding event. *J. Am. Chem. Soc.* **2005**, *127*, 5540–5551.

(21) Coelho, T.; Carvalho, M.; Saraiva, M. J.; Alves, I.; Almeida, M. R.; Costa, P. P. A strikingly benign evolution of FAP in an individual found to be a compound heterozygote for two TTR mutations: TTR Met 30 and TTR Met 119. *J. Rheumatol.* **1993**, *20*, 179.

(22) Coelho, T.; Chorao, R.; Sausa, A.; Alves, I.; Torres, M. F.; Saraiva, M. J. Compound heterozygotes of transthyretin Met30 and transthyretin Met119 are protected from the devastating effects of familial amyloid polyneuropathy. *Neuromuscular Disord.* **1996**, *6*, 27.

(23) Hammarstrom, P.; Schneider, F.; Kelly, J. W. *trans*-Suppression of misfolding in an amyloid disease. *Science* **2001**, *293*, 2459–2462.

(24) Miller, S. R.; Sekijima, Y.; Kelly, J. W. Native state stabilization by NSAIDs inhibits transthyretin amyloidogenesis from the most common familial disease variants. *Lab. Invest.* **2004**, *84*, 545–552.

(25) Johnson, S. M.; Petrassi, H. M.; Palaninathan, S. K.; Mohamedmohaideen, N. N.; Purkey, H.; Nichols, C.; Chiang, K. P.; Walkup, T.; Sacchettini, J. C.; Sharpless, K. B.; Kelly, J. W. Bisaryloxime ethers as potent inhibitors of transthyretin amyloid fibril formation. *J. Med. Chem.* **2005**, *48*, 1576–1587.

(26) Miroy, G. J.; Lai, Z.; Lashuel, H. A.; Peterson, S. A.; Strang, C.; Kelly, J. W. Inhibiting transthyretin amyloid fibril formation via protein stabilization. *Proc. Natl. Acad. Sci. U.S.A.* **1996**, *93*, 15051–15056.

(27) Oza, V. B.; Petrassi, H. M.; Purkey, H. E.; Kelly, J. W. Synthesis and evaluation of anthranilic acid-based transthyretin amyloid fibril inhibitors. *Bioorg. Med. Chem. Lett.* **1999**, *9*, 1–6.

(28) Oza, V. B.; Smith, C.; Raman, P.; Koepf, E. K.; Lashuel, H. A.; Petrassi, H. M.; Chiang, K. P.; Powers, E. T.; Sachettinni, J.; Kelly, J. W. Synthesis, structure, and activity of diclofenac analogues as

transthyretin amyloid fibril formation inhibitors. *J. Med. Chem.* **2002**, *45*, 321–332.
(29) Baures, P. W.; Peterson, S. A.; Kelly, J. W. Discovering transthyretin amyloid fibril inhibitors by limited screening. *Bioorg. Med. Chem.* **1998**, *6*, 1389–1401.
(30) Baures, P. W.; Oza, V. B.; Peterson, S. A.; Kelly, J. W. Synthesis and evaluation of inhibitors of transthyretin amyloid formation based on the non-steroidal anti-inflammatory drug, flufenamic acid. *Bioorg. Med. Chem.* **1999**, *7*, 1339–1347.
(31) Adamski-Werner, S. L.; Palaninathan, S. K.; Sacchettini, J. C.; Kelly, J. W. Diflunisal analogues stabilize the native state of transthyretin. Potent inhibition of amyloidogenesis. *J. Med. Chem.* **2004**, *47*, 355–374.
(32) Purkey, H. E.; Palaninathan, S. K.; Kent, K. C.; Smith, C.; Safe, S. H.; Sacchettini, J. C.; Kelly, J. W. Hydroxylated polychlorinated biphenyls selectively bind transthyretin in blood and inhibit amyloidogenesis: Rationalizing rodent PCB toxicity. *Chem. Biol.* **2004**, *11*, 1719–1728.
(33) Razavi, H.; Palaninathan, S. K.; Powers, E. T.; Wiseman, R. L.; Purkey, H. E.; Mohamedmohaideen, N. N.; Deechongkit, S.; Chiang, K. P.; Dendle, M. T.; Sacchettini, J. C.; Kelly, J. W. Benzoxazoles as transthyretin amyloid fibril inhibitors: synthesis, evaluation, and mechanism of action. *Angew. Chem., Int. Ed.* **2003**, *42*, 2758–2761.
(34) Razavi, H.; Powers, E. T.; Purkey, H. E.; Adamski-Werner, S. L.; Chiang, K. P.; Dendle, M. T.; Kelly, J. W. Design, synthesis, and evaluation of oxazole transthyretin amyloidogenesis inhibitors. *Bioorg. Med. Chem. Lett.* **2005**, *15*, 1075–1078.
(35) Petrassi, H. M.; Klabunde, T.; Sacchettini, J. C.; Kelly, J. W. Structure-based design of *N*-phenyl phenoxazine transthyretin amyloid fibril inhibitors. *J. Am. Chem. Soc.* **2000**, *122*, 2178–2192.
(36) Petrassi, H. M.; Johnson, S. M.; Purkey, H.; Chiang, K. P.; Walkup, T.; Jiang, X.; Powers, E. T.; Kelly, J. W. Potent and selective structure-based dibenzofuran inhibitors of transthyretin amyloidogenesis: Kinetic stabilization of the native state. *J. Am. Chem. Soc.* **2005**, *127*, 6662–6671.
(37) Purkey, H. E.; Dorrell, M. I.; Kelly, J. W. Evaluating the binding selectivity of transthyretin amyloid fibril inhibitors in blood plasma. *Proc. Natl. Acad. Sci. U.S.A.* **2001**, *98*, 5566–5571.
(38) Glenner, G. G. Amyloid deposits and amyloidosis: the beta-fibrilloses (second of two parts). *N. Engl. J. Med.* **1980**, *302*, 1333–1343.
(39) Kumar, D.; Jacob, M. R.; Reynolds, M. B.; Kerwin, S. M. Synthesis and evaluation of anticancer benzoxazoles and benzimidazoles related to UK-1. *Bioorg. Med. Chem.* **2002**, *10*, 3997–4004.
(40) Colon, W.; Kelly, J. W. Partial denaturation of transthyretin is sufficient for amyloid fibril formation in vitro. *Biochemistry* **1992**, *31*, 8654–8660.
(41) Hurshman, A. R.; White, J. T.; Powers, E. T.; Kelly, J. W. Transthyretin aggregation under partially denaturing conditions is a downhill polymerization. *Biochemistry* **2004**, *43*, 7365–7381.
(42) Glaser, K.; Sung, M. L.; O'Neill, K.; Belfast, M.; Hartman, D.; Carlson, R.; Kreft, A.; Kubrak, D.; Hsiao, C. L.; Weichman, B. Etodolac selectively inhibits human prostaglandin G/H synthase 2 (PGHS-2) versus human PGHS-1. *Eur. J. Pharmacol.* **1995**, *281*, 107–111.
(43) Inoue, A.; Yamakawa, J.; Yukioka, M.; Morisawa, S. Filter-binding assay procedure for thyroid hormone receptors. *Anal. Biochem.* **1983**, *134*, 176–183.
(44) Andrea, T. A.; Cavalieri, R. R.; Goldfine, I. D.; Jorgensen, E. C. Binding of thyroid hormones and analogues to the human plasma protein prealbumin. *Biochemistry* **1980**, *19*, 55–63.
(45) Auffinger, P.; Hays, F. A.; Westhof, E.; Ho, P. S. Halogen bonds in biological molecules. *Proc. Natl. Acad. Sci. U.S.A.* **2004**, *101*, 16789–16794.
(46) Hilal, S. H.; Karickhoff, S. W.; Carreira, L. A. A rigorous test for SPARC's chemical reactivity models: Estimation of more than 4300 ionization pKa's. *Quant. Struct.-Act. Relat.* **1995**, *14*, 348–355.
(47) Mancini, J. A.; Riendeau, D.; Falgueyret, J. P.; Vickers, P. J.; O'Neill, G. P. Arginine 120 of prostaglandin G/H synthase-1 is required for the inhibition by nonsteroidal anti-inflammatory drugs containing a carboxylic acid moiety. *J. Biol. Chem.* **1995**, *270*, 29372–29377.
(48) Garavito, R. M.; Mulichak, A. M. The structure of mammalian cyclooxygenases. *Annu. Rev. Biophys. Biomol. Struct.* **2003**, *32*, 183–206.
(49) Picot, D.; Loll, P. J.; Garavito, R. M. The X-ray crystal structure of the membrane protein prostaglandin H2 synthase-1. *Nature* **1994**, *367*, 243–249.
(50) Bhattacharyya, D. K.; Lecomte, M.; Rieke, C. J.; Garavito, M.; Smith, W. L. Involvement of arginine 120, glutamate 524, and tyrosine 355 in the binding of arachidonate and 2-phenylpropionic acid inhibitors to the cyclooxygenase active site of ovine prostaglandin endoperoxide H synthase-1. *J. Biol. Chem.* **1996**, *271*, 2179–2184.
(51) Baxter, J. D.; Goede, P.; Apriletti, J. W.; West, B. L.; Feng, W.; Mellstrom, K.; Fletterick, R. J.; Wagner, R. L.; Kushner, P. J.; Ribeiro, R. C.; Webb, P.; Scanlan, T. S.; Nilsson, S. Structure-based design and synthesis of a thyroid hormone receptor (TR) antagonist. *Endocrinology* **2002**, *143*, 517–524.
(52) Wagner, R. L.; Apriletti, J. W.; McGrath, M. E.; West, B. L.; Baxter, J. D.; Fletterick, R. J. A structural role for hormone in the thyroid hormone receptor. *Nature* **1995**, *378*, 690–697.
(53) Wagner, R. L.; Huber, B. R.; Shiau, A. K.; Kelly, A.; Cunha Lima, S. T.; Scanlan, T. S.; Apriletti, J. W.; Baxter, J. D.; West, B. L.; Fletterick, R. J. Hormone selectivity in thyroid hormone receptors. *Mol. Endocrinol.* **2001**, *15*, 398–410.
(54) Scanlan, T. S.; Yoshihara, H. A.; Nguyen, N. H.; Chiellini, G. Selective thyromimetics: tissue-selective thyroid hormone analogs. *Curr. Opin. Drug Discovery Dev.* **2001**, *4*, 614–622.
(55) Weatherman, R. V.; Fletterick, R. J.; Scanlan, T. S. Nuclear-receptor ligands and ligand-binding domains. *Annu. Rev. Biochem.* **1999**, *68*, 559–581.
(56) Wiseman, R. L.; Green, N. S.; Kelly, J. W. Kinetic stabilization of an oligomeric protein under physiological conditions demonstrated by a lack of subunit exchange: Implications for transthyretin amyloidosis. *Biochemistry* **2005**, *44*, 9265–9274.
(57) McCammon, M. G.; Scott, D. J.; Keetch, C. A.; Greene, L. H.; Purkey, H. E.; Petrassi, H. M.; Kelly, J. W.; Robinson, C. V. Screening transthyretin amyloid fibril inhibitors: Characterization of novel multiprotein, multiligand complexes by mass spectrometry. *Structure* **2002**, *10*, 851–863.
(58) Lashuel, H. A.; Wurth, C.; Woo, L.; Kelly, J. W. The most pathogenic transthyretin variant, L55P, forms amyloid fibrils under acidic conditions and protofilaments under physiological conditions. *Biochemistry* **1999**, *38*, 13560–13573.
(59) Otwinowski, Z.; Minor, W. Processing of X-ray diffraction data collected in oscillation mode. *Methods Enzymol.* **1997**, *276*, 307–326.
(60) Green, N. S.; Palaninathan, S. K.; Sacchettini, J. C.; Kelly, J. W. Synthesis and characterization of potent bivalent amyloidosis inhibitors that bind prior to transthyretin tetramerization. *J. Am. Chem. Soc.* **2003**, *125*, 13404–13414.
(61) Storoni, L. C.; McCoy, A. J.; Read, R. J. Likelihood-enhanced fast rotation functions. *Acta Crystallogr., Sect. D: Biol. Crystallogr.* **2004**, *60* (Pt 3), 432–438.
(62) Murshudov, G. N.; Vagin, A. A.; Dodson, E. J. Refinement of macromolecular structures by the maximum-likelihood method. *Acta Crystallogr., Sect. D: Biol. Crystallogr.* **1997**, *53* (Pt 3), 240–255.
(63) Lovell, S. C.; Davis, I. W.; Arendall, W. B.3rd; de Bakker, P. I.; Word, J. M.; Prisant, M. G.; Richardson, J. S.; Richardson, D. C. Structure validation by Calpha geometry: phi,psi and Cbeta deviation. *Proteins* **2003**, *50* (3), 437–450.
(64) Vriend, G. WHAT IF: A molecular modeling and drug design program. *J. Mol. Graph.* **1990**, *8*, 52–56.
(65) Terwilliger, T. C. Automated main-chain model building by template matching and iterative fragment extension. *Acta Crystallogr., Sect. D: Biol. Crystallogr.* **2003**, *59* (Pt 1), 38–44.
(66) Laskowski, R.; MacArthur, M.; Moss, D.; Thornton, J. PROCHECK: A program to check the stereochemical quality of protein structures. *J. Appl. Crystallogr.* **1993**, *26*, 283–291.

JM0708735